A mixed spatial-spectral eddy-current formulation for pieces with one symmetry axis

Anastassios Skarlatos

▶ To cite this version:

Anastassios Skarlatos. A mixed spatial-spectral eddy-current formulation for pieces with one symmetry axis. IEEE Transactions on Magnetics, 2020, 56 (9), pp.1-11. 10.1109/TMAG.2020.3008092 . cea-04554320

HAL Id: cea-04554320
https://cea.hal.science/cea-04554320v1

Submitted on 13 Nov 2024

HAL is a multi-disciplinary open access archive for the deposit and dissemination of scientific research documents, whether they are published or not. The documents may come from teaching and research institutions in France or abroad, or from public or private research centers.

L'archive ouverte pluridisciplinaire **HAL**, est destinée au dépôt et à la diffusion de documents scientifiques de niveau recherche, publiés ou non, émanant des établissements d'enseignement et de recherche français ou étrangers, des laboratoires publics ou privés.

A mixed spatial-spectral eddy-current formulation for pieces with one symmetry axis

Anastassios Skarlatos, *Member, IEEE*
CEA LIST, CEA Saclay, F-91191 Gif-sur-Yvette, France

***Abstract*—A combination of the mesh-based finite integration technique with a modal expansion is proposed for the solution of the eddy-current induction problem in geometries involving work-pieces with translational or rotational symmetry and an arbitrary three-dimensional current excitation. The solution is expanded in a series of modes along the symmetry axis, and the thus reduced Helmholtz equation is discretised and solved independently for each mode in the transversal plane. Finally, the impedance variation of the eddy-current probe is evaluated by means of the reciprocity theorem. The main advantage of the proposed decomposition relies on the use of a two-dimensional instead of three-dimensional grid with the consequent reduction of the numerical noise, and the smaller size of the resulting linear system, which allows the simultaneous treatment of different sources.**

***Index Terms*—Nondestructive testing, eddy currents, finite difference methods, modal analysis.**

I. INTRODUCTION

EDDY-current fields are well localised around the driving inductor, which allows us to restrict the analysis in the vicinity of the sources, and consequently neglect, to a good approximation, what lies beyond. In eddy-current applications, in particular, this feature has been largely exploited in order to develop fast, semi-analytical solutions that apply to canonical geometries, which resemble, or at least locally approximate to a good extend, the specimen under consideration. The origin of these works lies to the seminal articles of Dodd and Deeds, who developed modal solutions for a number of infinite planar and cylindrical multilayer structures [1], [2]. Recent works, based on the truncation of the computational domain, have extended the applicability of the modal approach providing solution to canonical geometries which involved discontinuities. Theodoulidis and Bowler derived in [3] the solution near a half-space edge, and in [4] the analysis is extended to take into account thin cracks emanating from the edge. In [5]–[7] the similar problem of the fastener hole, with and without defect, is tackled. Combining modal expansions in different coordinate systems, more complex geometries, consisting of a number of different canonical parts can be tackled, such as an infinitely long pipe embedded in a conducting substrate [8], or a buried hollow sphere [9], [10]. An important advantage of these approaches, beside their speed, is that they can provide explicit expressions of the Green dyadic operator, which applied as dedicated kernel in an integral equation formulation provides a very efficient and precise computation of the eddy-current response of small defects [4], [7].

In the modal approach referred to above, the development basis is constructed in the spectral domain, which has to be an eigenbasis of the Helmholtz operator, in at least one subdomain of the structure, in order to obtain a sparse system matrix (or partially sparse when mode-matching comes into play). Such a basis cannot be constructed in the general case except for a number of canonical geometries like the ones treated in the above cited works. In the more general case, one has to work instead directly in the spatial domain, introducing a discrete basis of local elements, where however the demand of diagonalisation of the Helmholtz operator is abandoned. This is the case in volume-mesh-based methods like the finite element method (FEM) [11]–[14] or the dinite differences (FD) / finite integration technique (FIT) [15]–[18], where sparsity (yet not diagonality) is maintained for the three spatial directions. Alternatively, one can scarify the sparsity in favour of dimensionality reduction by restricting the basis support on the geometry interfaces and employing an analytical free-space operator to provide the solution inside the piece volume. This approach yields the family of the boundary elements method (BEM) [19], which can be interesting when where are dealing with piece-wise homogeneous materials with relatively smooth interfaces. The constrain of piecewise homogeneity can be relaxed though if a volume-mesh in the interior of the non-homogeneous conducting/magnetic pieces is employed [20]–[25].

The present work is positioned between the two extreme cases, namely between configurations involving solely canonical pieces and those with completely arbitrary geometries. More precisely, we shall consider pieces presenting translational or rotational symmetry and arbitrary profile on the transversal (to the symmetry axis) plane. We shall make instead no particular assumption concerning the form of the excitation current. The analysis will be restricted to the low frequency regime, i.e., it is valid only in the quasi-static limit of the full Maxwell equations. It turns out that the problems satisfying the above assumptions are neither two-dimensional nor purely three-dimensional since the pieces present an axis of invariance the source field being three-dimensional. We shall thus refer to this problem from this point forth as the 2.5 dimensional problem.

Taking advantage of the geometry invariance along the third dimension, the solution is expanded in a modal basis along that axis, decoupling the initial 3D problem to a number of independent 2D problems, one for each mode. The calculation of the field profile for each of the modes is carried out via a FIT discretisation scheme on the transversal plane. The idea of modal decomposition has already been applied for calculations in source-free waveguides and resonant cavities [26]. Herein, this principle is extended in order to take into account arbitrary sources. The introduction of current sources in the discretisation scheme is significantly simplified by decomposing the field in the air in a free-space source term and a scattering term and expressing the former by means of an equivalent current distribution on a closed surface according to the Huygens principle [27]. Finally, the variation of the eddy-current probe impedance, a measurement of practical interest, can be easily obtained by application of the reciprocity theorem [28].

The interest in applying the proposed indirect analysis is twofold. Reducing the spatial discretisation from 3D to 2D is very beneficial in terms of the mesh simplicity and the thereto related numerical noise. Meanwhile, the decomposition of the initial 3D problem to a number of separate 2D problems of much smaller size allows the application of direct solvers for the inversion of the resulting algebraic system of equation, which proves to be an important advantage when the problem has to be solved for a number of different excitations such as the case of a moving (scanning) coil. This feature is particularly interesting for addressing eddy-current non-destructive evaluation situations, where a complete scan of the sensing coil above the inspected specimen has to be taken into account. In addition, the problem becomes easily parallelizable since each mode is independent from all the others.

The paper is organised as follows. The FIT-modal formulation is derived in section II. The necessary gauging of the curl-curl equation is also examined in order to cope with the indefiniteness of the operator in air regions. In section III, the source term is constructed on the basis of the induction equivalent theorem. The calculation of the impedance variation during to the presence of the piece is given in section IV. Finally, the results obtained with the proposed formulation are compared against reference semi-analytical solutions as well as experimental data in section V. The article is concluded with a discussion on the results and the possible extensions of this work.

II. MIXED FIT-MODAL FORMULATION IN GEOMETRIES WITH TRANSLATIONAL OR ROTATIONAL INVARIANCE

A. The Maxwell grid equations

In the classical FIT formulation, Maxwell's equations are discretised in a pair of mutually orthogonal, staggered grids, referred to as primary grid G and dual grid $\widetilde{G}$, respectively, leading to a system of matrix equations, the so-called Maxwell grid equations [15]. Assuming harmonic excitation of the form $e^{j\omega t}$, where ω is the angular frequency, and considering linear materials, the latter admit the following form [16], [17], [27]:

$$\mathbf{C}\widehat{\mathbf{e}} = -j\omega\widehat{\widehat{\mathbf{b}}} - \widehat{\widehat{\mathbf{j}}}_m \tag{1}$$

$$\widetilde{\mathbf{C}}\widehat{\mathbf{h}} = j\omega\widehat{\widehat{\mathbf{d}}} + \widehat{\widehat{\mathbf{j}}}_e \tag{2}$$

$$\widetilde{\mathbf{S}}\widehat{\widehat{\mathbf{d}}} = \mathbf{q}_e \tag{3}$$

$$\mathbf{S}\widehat{\widehat{\mathbf{b}}} = \mathbf{0} \tag{4}$$

where $\widehat{\mathbf{e}}$, $\widehat{\mathbf{h}}$ are column vectors composed by the electric and magnetic field integrals along the primary and dual grid edges, whereas $\widehat{\widehat{\mathbf{d}}}$ and $\widehat{\widehat{\mathbf{b}}}$ stand for the electric and magnetic flux across the primary and dual grid facets, respectively. Similarly, $\widehat{\widehat{\mathbf{j}}}_e$ and $\widehat{\widehat{\mathbf{j}}}_m$ stand for the discretised electric and magnetic current fluxes across the primary and dual grid facets, and $\mathbf{q}_e$ are the corresponding electric charges contained in the primary grid cells. The reason for including the non-physical magnetic current term $\widehat{\widehat{\mathbf{j}}}_m$ in the Maxwell equations will become clear at a latter point, where we shall separate the source field term from the rest of the solution [27].

The $\mathbf{C}, \widetilde{\mathbf{C}}$ matrices stand for the curl operator in the primary and dual grid space, respectively. They are interrelated via the duality property $\widetilde{\mathbf{C}} = \mathbf{C}^T$. In the same fashion, $\mathbf{S}$ and $\widetilde{\mathbf{S}}$ matrices form the corresponding discrete div operators acting upon the two grid-related variables, and which retain the topological structure of their continuous counterparts, namely

$$\mathbf{SC} = \mathbf{0}. \tag{5}$$

The analogous relation exists also for the dual-grid operators.

It proves useful to introduce also the discrete grad operator $\mathbf{G}$, which satisfies the corresponding vector identity

$$\mathbf{CG} = \mathbf{0}. \tag{6}$$

Notice that $\mathbf{S}$ and $\mathbf{G}$ are related via $\mathbf{G} = -\widetilde{\mathbf{S}}^T$. The identity expressed by (6) guaranties a divergence free magnetic induction when no magnetic free charges exist in the computational domain as it can be easily shown by direct application in (4) for $\mathbf{q}_m = 0$.

The above described numerical scheme is completed by introducing the constitutive material relations, which in the discrete space of the dual grid system read

$$\widehat{\widehat{\mathbf{d}}} = \mathbf{M}_\varepsilon\widehat{\mathbf{e}} \tag{7}$$

$$\widehat{\widehat{\mathbf{b}}} = \mathbf{M}_\mu\widehat{\mathbf{h}} \tag{8}$$

$$\widehat{\widehat{\mathbf{j}}}_{ec} = \mathbf{M}_\kappa\widehat{\mathbf{e}} \tag{9}$$

where $\widehat{\widehat{\mathbf{j}}}_{ec}$ gives for the eddy-current contribution to the total electric current term $\widehat{\widehat{\mathbf{j}}}_e$, and the diagonal matrices $\mathbf{M}_\varepsilon$, $\mathbf{M}_\mu$ and $\mathbf{M}_\kappa$ stand for the electric permittivity, magnetic permeability and electric conductivity matrices respectively. For a detailed description of their structure and their construction the reader is referred to [16], [17].

From this point forward, we shall consider the quasi-static limit of the Maxwell equations, i.e. the frequency will be assumed sufficiently low in order to ignore the displacement current term $j\omega\widehat{\widehat{\mathbf{d}}}$.

B. Modal Expansion of the Solution Along the Direction of Symmetry

Let us consider a configuration consisting of a translationally or rotationally symmetric work-piece and an arbitrary, current distribution. The two cases are conveniently addressed in the context of the FIT discretisation scheme by a Cartesian and a cylindrical grid system, respectively. The two grid systems and the corresponding allocation schemes for the electric $\widehat{\mathbf{e}}$ and magnetic fields $\widehat{\mathbf{h}}$ are shown in Fig. 2. The corresponding fluxes $\widehat{\widehat{\mathbf{d}}}, \widehat{\widehat{\mathbf{b}}}$ and currents $\widehat{\widehat{\mathbf{j}}}_e, \widehat{\widehat{\mathbf{j}}}_m$ are allocated

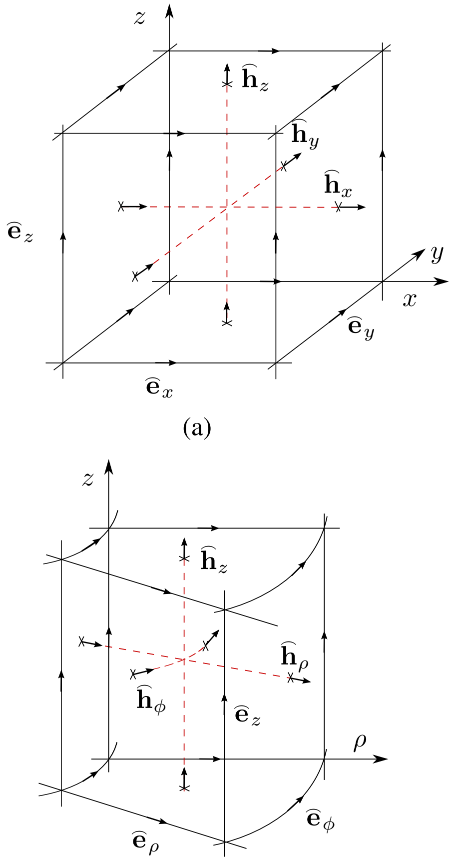

(a)

(b)

Fig. 1. FIT dual grid system for the two considered coordinate systems: (a) Cartesian and (b) cylindrical.

in the same positions with the electric and magnetic fields respectively.

Let y and ϕ be the axis of invariance for the translationally and rotationally symmetric case, respectively. In order to better exploit the isomorphism of the transversal plane for the two grid systems, namely the $x-z$ plane for the Cartesian and $\rho-z$ plane for the cylindrical one, a generic coordinate system (u, v, w) is introduced, which is defined in the following way. Let w be the symmetry axis in both cases. u and v are assigned to the remaining two axes in a way that they satisfy the right hand rule, namely $\hat{\mathbf{u}} \times \hat{\mathbf{v}} = \hat{\mathbf{w}}$ (and the thereupon cyclic permutations), where $\hat{\mathbf{u}}, \hat{\mathbf{v}}, \hat{\mathbf{w}}$ stand for the unit vectors in u, v and w direction, respectively. Hence we obtain the transformation rule, $(x, y, z) \to (u, -w, v)$ for the Cartesian system and $(\rho, \phi, z) \to (u, -w, v)$ for the cylindrical one. Using the thus defined coordinate system, the same relations will apply hereafter indistinguishably for the two symmetries.

Following the common practice in low-frequency applications, we shall assume that the induced field is negligible at sufficient distances from the source, and hence we shall truncate the computational domain at $\pm L$ in case of the Cartesian system, using a perfectly electric conductor (PEC) or perfectly magnetic conductor (PMC) condition. The use of either PEC of PMC termination implies periodicity of the solution along the truncation direction, which, given L sufficiently large, does not introduce significant aliasing in the region of interest. The truncation limit L is determined based on geometrical criteria, the conductivity of the piece and the inspection frequency; thorough studies on their estimation exist in the literature [3], and thus their values will be considered as known in this work. For the cylindrical case, the periodicity of the solution is naturally imposed $\phi = 2\pi$ boundary [5], [6], [9].

Making use of the above periodicity and taking into account the invariance of the geometry along w, we can expand all state variables in terms of an exponential Fourier series along that direction as follows:

$$\mathbf{x}(u, v, w) = \sum_{n=-\infty}^{\infty} \mathbf{x}_n(u, v)\, e^{j\kappa_n w}, \tag{10}$$

with $\kappa_n = n\pi/L$ for translational and $\kappa_n = n$ for rotational symmetry, respectively. Practically, the above sum is limited to a finite number of modes N, which depends upon the details of the configuration. In most cases, (10) converges rapidly, thus a number of modes of few tens delivers a very satisfactory precision [3], [5]–[9].

C. Discretisation on the transversal plane

We apply the (10) expansion to the FIT state variables $\widehat{\mathbf{e}}, \widehat{\mathbf{h}}, \widehat{\widehat{\mathbf{b}}}, \widehat{\widehat{\mathbf{j}}}_e$ and $\widehat{\widehat{\mathbf{j}}}_m$, and we derive the Maxwell grid equations on a FIT grid doublet $\{G, \widetilde{G}\}$ consisting of a single cell along the w direction, centred at $w = 0$ (cf. Fig. 2). Note here, that the variation along the w direction is taken into account be means of (10), the finite cell size Δw along the w direction, is merely used for mathematical convenience and numerical stability.

Let us consider the calculation of the state variables at an arbitrary cell i, whose $u-w$ plane section is shown in Fig. 2. For the sake of brevity we shall restrict the analysis to the $\widehat{\mathbf{e}}$, $\widehat{\widehat{\mathbf{b}}}$ variables only. The same calculations apply for the remaining variables $\widehat{\mathbf{h}}$, $\widehat{\widehat{\mathbf{j}}}_e$ and $\widehat{\widehat{\mathbf{j}}}_m$.

From the geometry of the grids and the FIT allocation system it is clear that the $\widehat{e}_{u,i}$, $\widehat{e}_{v,i}$ and $\widehat{\widehat{b}}_{w,i}$ elements need to be calculated at $w = -\Delta w/2$, which yields for these variables

$$\left\{ \begin{matrix} \widehat{e}_{u,v;i}(-\Delta w/2) \\ \widehat{\widehat{b}}_{w;i}(-\Delta w/2) \end{matrix} \right\} = \sum_{n=-\infty}^{\infty} \left\{ \begin{matrix} \widehat{\mathbf{e}}_{u,v;in} \\ \widehat{\widehat{\mathbf{b}}}_{w;in} \end{matrix} \right\} \exp(-j\kappa_n \Delta w/2)\,. \tag{11}$$

The $e_{w;i}$ element is integrated along the $[-\Delta w/2, \Delta w/2]$ integral, which means

$$\begin{aligned} \widehat{e}_{w;i}(0) &= \sum_{n=-\infty}^{\infty} e_{w;in} \int_{-\Delta w/2}^{\Delta w/2} e^{j\kappa_n w} dw \\ &= \sum_{n=-\infty}^{\infty} e_{w;in} \Delta w \mathrm{sinc}(\kappa_n w) \end{aligned} \tag{12}$$

In the same fashion we obtain for the $\widehat{\widehat{b}}_{u;in}$, $\widehat{\widehat{b}}_{v;in}$ fluxes

$$\left\{ \begin{matrix} \widehat{\widehat{b}}_{u;i}(0) \\ \widehat{\widehat{b}}_{v;i}(0) \end{matrix} \right\} = \sum_{n=-\infty}^{\infty} \left\{ \begin{matrix} \int_{\Delta v_i} b_{u;n}(v)\, dv \\ \int_{\Delta v_i} b_{v;n}(u)\, du \end{matrix} \right\} \Delta w \mathrm{sinc}(\kappa_n w) \tag{13}$$

with $\Delta_{v;i}\Delta w$, $\Delta_{u;i}\Delta w$ standing for the respective facets areas. Note that the metric of the grid is implicitly taken into account via the integration along the corresponding grid elements. Hence, in the case of a cylindrical grid, the u integrals are carried out along the corresponding arcs $u_i\Delta w$ (recall that the w coordinate in the cylindrical coordinate system is the azimuthal angle ϕ).

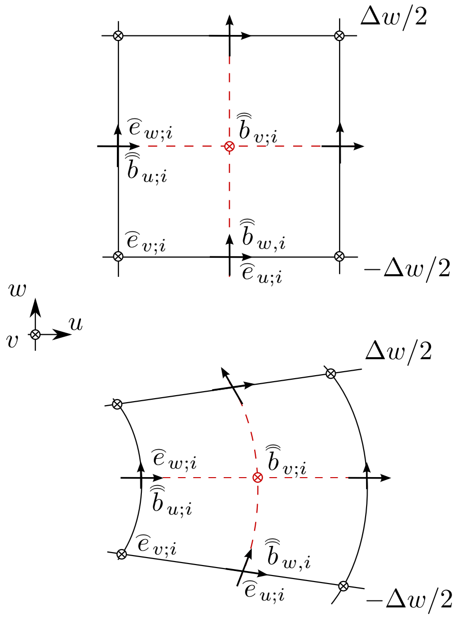

Fig. 2. Grid section on the $u-w$ plane for the two coordinate systems. The $\widehat{\mathbf{e}}_u$, $\widehat{\mathbf{e}}_v$ and $\widehat{\widehat{\mathbf{b}}}_w$ elements are calculated at the $\pm\Delta w/2$ positions whereas $\widehat{\mathbf{e}}_w$, $\widehat{\widehat{\mathbf{b}}}_u$ and $\widehat{\widehat{\mathbf{b}}}_v$ need to be integrated in the $[-\Delta w/2, \Delta w/2]$ interval. i stands for the cell index.

In order to comply with the ordinary FIT conventions, we define

$$\widehat{e}_{w;in} := x_{w;in}\Delta w \tag{14}$$

and

$$\widehat{\widehat{b}}_{t;in} := \left\{ \begin{array}{c} \int\limits_{\Delta v_i} b_{u;n}(v)\,dv \\ \int\limits_{\Delta v_i} b_{v;n}(u)\,du \end{array} \right\} \Delta w. \tag{15}$$

Notice that the thus defined integrated state variables differ from their exact values, which are obtained after multiplication with the $\mathrm{sinc}(\kappa\Delta w/2)$ term. The reason for this definition (which has however no impact to the accuracy of the method) is the elimination of the $\mathrm{sinc}(.)$ terms from the discrete equations. Once the values of the integrated variables are known, we can obtain at any moment the exact value by restoring the sinc term.

Using the above conventions, the Maxwell grid equations take the following form in the spatial-spectral domain

$$\left(\mathbf{C}_t + j\alpha_n\mathbf{J}\right)\widehat{\mathbf{e}} = -j\omega\widehat{\widehat{\mathbf{b}}} - \widehat{\widehat{\mathbf{j}}}_m \tag{16}$$

$$\left(\widetilde{\mathbf{C}}_t + j\alpha_n\mathbf{J}\right)\widehat{\mathbf{h}} = \widehat{\widehat{\mathbf{j}}}_e \tag{17}$$

$$\left(\widetilde{\mathbf{S}}_t + j\alpha_n\mathbf{E}\right)\widehat{\widehat{\mathbf{d}}} = \mathbf{q}_e \tag{18}$$

$$\left(\mathbf{S}_t + j\alpha_n\mathbf{E}\right)\widehat{\widehat{\mathbf{b}}} = \mathbf{0} \tag{19}$$

with $\alpha_n = \kappa_n\Delta_w$. $\mathbf{C}_t$ and $\mathbf{S}_t$ stand for the transversal curl and div primary gird operators, given by

$$\mathbf{C}_t = \begin{pmatrix} \mathbf{0} & \mathbf{0} & \mathbf{P}_v \\ \mathbf{0} & \mathbf{0} & -\mathbf{P}_u \\ -\mathbf{P}_v & \mathbf{P}_u & \mathbf{0} \end{pmatrix} \tag{20}$$

and

$$\mathbf{S}_t = \begin{pmatrix} \mathbf{P}_u & \mathbf{P}_v & \mathbf{0} \end{pmatrix} \tag{21}$$

whereas $\mathbf{J}$ and $\mathbf{E}$ are unit matrices

$$\mathbf{J} = \begin{pmatrix} \mathbf{0} & -\mathbf{I} & \mathbf{0} \\ \mathbf{I} & \mathbf{0} & \mathbf{0} \\ \mathbf{0} & \mathbf{0} & \mathbf{0} \end{pmatrix} \tag{22}$$

and

$$\mathbf{E} = \begin{pmatrix} \mathbf{0} & \mathbf{0} & \mathbf{I} \end{pmatrix} \tag{23}$$

and $\mathbf{P}_{u,v}$ sub-matrices stand for the discrete differentiation operators along the two coordinate axes of the $u-v$ plane. Their detailed expressions are given in [17]. The corresponding relations for the dual-grid matrices are obtained by applying the duality principle given above. Since the spatial dependence along the normal w axis has been absorbed by the modal expansion terms, there is no need to refer to the initial single w-cell 3D grid, the planar grid system depicted in Fig. 3 being more appropriate for the analysis.

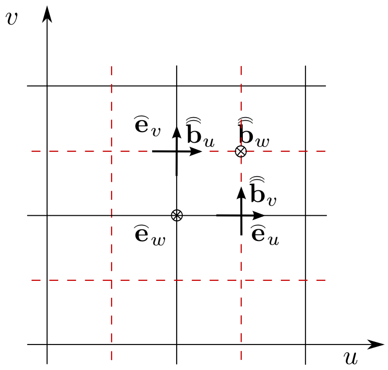

Fig. 3. Two dimensional grid on the $u-v$ plane after application of the modal expressions.

Eliminating $\widehat{\mathbf{h}}$, $\widehat{\widehat{\mathbf{b}}}$ from the Maxwell grid equations (16),(17) taking into account the constitutive relations (8),(9) yields the following discrete curl-curl equation for the mode n

$$\left(\mathbf{A}_n + j\omega\mathbf{M}_\kappa\right)\widehat{\mathbf{e}}_n = -j\omega\widehat{\widehat{\mathbf{j}}}_{e,n} - \left(\widetilde{\mathbf{C}}_t + j\alpha_n\mathbf{J}\right)\mathbf{M}_\mu^{-1}\widehat{\widehat{\mathbf{j}}}_{m,n}. \tag{24}$$

with

$$\begin{aligned}\mathbf{A}_n = {} & \widetilde{\mathbf{C}}_t\mathbf{M}_\mu^{-1}\mathbf{C}_t + j\alpha_n\left(\widetilde{\mathbf{C}}_t\mathbf{M}_\mu^{-1}\mathbf{J} + \mathbf{J}\mathbf{M}_\mu^{-1}\mathbf{C}_t\right) \\ & - \alpha_n^2\mathbf{J}\mathbf{M}_\mu^{-1}\mathbf{J}. \end{aligned} \tag{25}$$

It is interesting to derive the explicit formulations of the different matrix terms in the curl-curl equation (24) in order to get insight to the physical interpretation of the different terms. Hence, one can show

$$\widetilde{\mathbf{C}}_t\mathbf{M}_\mu^{-1}\mathbf{C}_t = \begin{pmatrix} \mathbf{P}_v^T\mathbf{M}_w\mathbf{P}_v & -\mathbf{P}_v^T\mathbf{M}_w\mathbf{P}_u & \mathbf{0} \\ -\mathbf{P}_u^T\mathbf{M}_w\mathbf{P}_v & \mathbf{P}_u^T\mathbf{M}_w\mathbf{P}_u & \mathbf{0} \\ \mathbf{0} & \mathbf{0} & \mathbf{P}_v^T\mathbf{M}_u\mathbf{P}_v + \mathbf{P}_u^T\mathbf{M}_v\mathbf{P}_u \end{pmatrix} \quad (26)$$

$$\widetilde{\mathbf{C}}_t\mathbf{M}_\nu\mathbf{J} + \mathbf{J}\mathbf{M}_\nu\mathbf{C}_t = \begin{pmatrix} \mathbf{0} & \mathbf{0} & \mathbf{M}_v\mathbf{P}_u \\ \mathbf{0} & \mathbf{0} & \mathbf{M}_u\mathbf{P}_v \\ \mathbf{P}_u^T\mathbf{M}_v & \mathbf{P}_v^T\mathbf{M}_u & \mathbf{0} \end{pmatrix} \quad (27)$$

and

$$\mathbf{J}\mathbf{M}_u\mathbf{J} = -\begin{pmatrix} \mathbf{M}_v & \mathbf{0} & \mathbf{0} \\ \mathbf{0} & \mathbf{M}_u & \mathbf{0} \\ \mathbf{0} & \mathbf{0} & \mathbf{0} \end{pmatrix}. \quad (28)$$

where $\mathbf{M}_u, \mathbf{M}_v$ and $\mathbf{M}_w$ are the submatrices of the inverse magnetic permeability (reluctivity) matrix along the u, v and w directions, respectively. The two non-zero clusters lumped around the main matrix diagonal in (26) and (28) stand for the TE$_w$ and TM$_w$ parts of the curl-curl operator. The TE$_w$ and TM$_w$ solutions are coupled via the (27) submatrix. Clearly for $a_n = 0$, the two solutions are independent, which reproduces the theoretical result of the TE$_w$ and TM$_w$ uncoupling in the 2D case.

D. Gauging

When applied to non-conducting regions, (24) leads to not unique solutions since any term of the form $-\mathbf{G}\psi$, with ψ an arbitrary scalar potential, belongs to the null-space of the curl-curl operator, as it can be easily verified using the identity (6). This is a well known issue in low-frequency electromagnetic problems, and a number of different gauging strategies has been proposed in the literature to address it, the tree-cotree formulation being a well established techniques [21], [29]. Yet, the matrix structure of the FIT discretisation scheme offers a simple way of gauging, based on the subtraction of a rotational-free operator, which offers the additional advantage of a direct physical interpretation [30]. A more elaborated scheme, better suited for the quasi-static regime, has been proposed Clemens et al. [31], [32] for the FIT formulation, where a similar approach with the one proposed by Bossavit for the FEM method [33] is adopted. It is interesting to note the that in the air regions, the previous approach reduce to a regularisation term similar to the one proposed by Biro and Preis [34].

In this work, a simplified version of the regularisation matrix of [31], [32] has been used, in the sense that the gauging matrix is restricted in the air-regions (which makes it also equivalent with that of [34]) and by the substitution of the scaling matrix $\mathbf{M_2}$ by a scalar coefficient equal to its minimum value, namely

$$\frac{r}{\mu_0\varepsilon_0^2 \max D_{\tilde{V}}}\mathbf{M}_\varepsilon\mathbf{G}\widetilde{\mathbf{S}}\mathbf{M}_\varepsilon \quad (29)$$

with $D_{\tilde{V}}$ standing for the diagonal matrix of the dual cells volumes and r being an optional relaxation factor (in this work we set $r = 1$). Note that the $1/\mu_0\varepsilon_0^2$ factor scales the matrix values to the free-space reluctivity (in accordance with [34] and [31], [32]), the $\mathbf{M}_\varepsilon$ term on the left realises the mapping of electric voltages to the electric flux density and hence assures the metric consistency, and the $\mathbf{M}_\varepsilon$ factor on the left restores the symmetry of the matrix. Finally the cell volume factor balances the gauge term metric with that of the curl-curl matrix.

Substituting (21) taking into account the definition of $\mathbf{G}$, the grad-div operator $\mathbf{G}\widetilde{\mathbf{S}}$ can be decomposed in three terms in the same fashion with curl-curl operator

$$\mathbf{G}\widetilde{\mathbf{S}} = -\widetilde{\mathbf{S}}_t^T\widetilde{\mathbf{S}}_t - j\alpha_n\left(\widetilde{\mathbf{S}}_t^T\mathbf{E} + \mathbf{E}^T\widetilde{\mathbf{S}}_t\right) - \alpha_n^2\mathbf{E}^T\mathbf{E} \quad (30)$$

with the submatrices $\mathbf{G}_t\widetilde{\mathbf{S}}_t$, $\mathbf{G}_t\mathbf{E} + \mathbf{E}^T\widetilde{\mathbf{S}}_t$ and $\mathbf{E}^T\mathbf{E}$ given by

$$\widetilde{\mathbf{S}}_t^T\widetilde{\mathbf{S}}_t = \begin{pmatrix} \mathbf{P}_u\mathbf{P}_u^T & \mathbf{P}_u\mathbf{P}_v^T & \mathbf{0} \\ \mathbf{P}_v\mathbf{P}_u^T & \mathbf{P}_v\mathbf{P}_v^T & \mathbf{0} \\ \mathbf{0} & \mathbf{0} & \mathbf{0} \end{pmatrix} \quad (31)$$

$$\widetilde{\mathbf{S}}_t^T\mathbf{E} - \mathbf{E}^T\widetilde{\mathbf{S}}_t = \begin{pmatrix} \mathbf{0} & \mathbf{0} & \mathbf{P}_u \\ \mathbf{0} & \mathbf{0} & \mathbf{P}_v \\ \mathbf{P}_u^T & \mathbf{P}_v^T & \mathbf{0} \end{pmatrix} \quad (32)$$

and

$$\mathbf{E}^T\mathbf{E} = \begin{pmatrix} \mathbf{0} & \mathbf{0} & \mathbf{0} \\ \mathbf{0} & \mathbf{0} & \mathbf{0} \\ \mathbf{0} & \mathbf{0} & -\mathbf{I} \end{pmatrix}. \quad (33)$$

III. MODELLING OF THE SOURCES: APPLICATION OF THE EQUIVALENCE THEOREM

According to our basic hypothesis, the current sources are arbitrary, with the only restriction that they must be solenoidal, i.e. they must satisfy the condition

$$\nabla \cdot \mathbf{J}_s = 0 \quad (34)$$

or equivalently in the FIT basis

$$\widetilde{\mathbf{S}}\widehat{\widehat{\mathbf{j}}}_s = 0 \quad (35)$$

in order to be consistent with the magneto-quasi-static approximation.

In reality, the current sources involved in the majority of practical eddy current applications are coils of several shapes, which are allowed to change position and orientation during a scan. The straight forward approach to handle the excitation currents is to project the (known) current density $\mathbf{J}_s$ in the expansion basis (10) along the w axis, and to discretize the thus obtained cross-sectional density $\mathbf{J}_n$ for each mode in order to obtain the excitation vectors $\widehat{\widehat{\mathbf{j}}}_{e,n}$. Nevertheless, this approach is cumbersome and the accuracy of the current discretisation is dependent on the grid refinement at the coils location and for every scan position. In other words, we are facing again the same problem we wish to alleviate from the very beginning of this approach, namely the strong dependence from the grid resolution.

A more elegant and efficient approach which allows us to relax the constrains for the grid resolution is to transform the initial problem into an equivalent one, where the excitation sources bear a simpler geometrical form, conformal to the symmetry of the piece. This approach is based on the equivalence principle, in particular, the formulation known as the induction equivalent [35]. The quintessence of the theorem

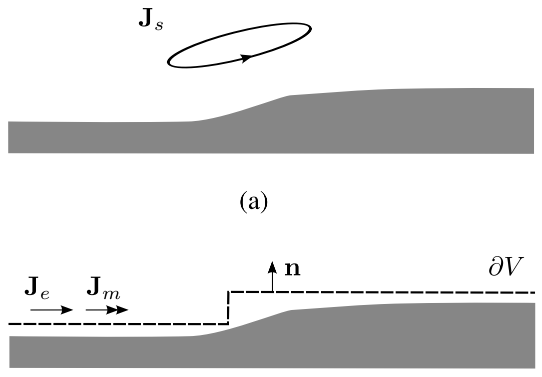

(a)

(b)

Fig. 4. Construction of the equivalent problem: (a) original configuration, (b) equivalent problem with electric and magnetic surface currents. The boundary surface is indicated by the dotted line, and is assumed to be closing in the infinity.

consists in the introduction of a fictitious closed boundary ∂V, which entirely encloses the conducting piece, and the subsequent replacement of the initial volumetric electric current source by surface electric and a surface magnetic sources on ∂V. The new problem is equivalent with the original one in the interior of the boundary ∂V, which will be called henceforth as the Huygens surface for brevity. A schematic representation of the equivalence principle is shown in Fig. 4.

Let $\mathbf{E}_0$ and $\mathbf{H}_0$ be, the electric and magnetic field induced by the current source in the absence of the work-piece. The equivalent sources are then defined via the relations

$$\mathbf{J}_e = \mathbf{n} \times \mathbf{H}_0 \tag{36}$$

$$\mathbf{J}_m = -\mathbf{n} \times \mathbf{E}_0, \tag{37}$$

$\mathbf{n}$ being the outwards pointing unit normal to ∂V. For the sake of simplicity, we shall consider only the first equation for a Huygens surface normal to the v axis, at $v = v_s$. The analysis for the u axis and the magnetic current density is analogous. The equivalent electric current density obtain by the application of the definition relation (36) reads

$$\begin{pmatrix} J_{e,u}(u,v) \\ J_{e,v}(u,v) \\ J_{e,w}(u,v) \end{pmatrix} = \begin{pmatrix} H_w(u,v_s) \\ 0 \\ -H_u(u,v_s) \end{pmatrix} \delta(v - v_S) \tag{38}$$

where it is recalled that all the quantities are understood as the projections of the corresponding spatial functions to the mode $e^{j\kappa_n w}$. The delta function on the right hand side of the equation stems from the fact that the equivalent current distribution has by definition zero thickness. In order to obtain from (38) the respective FIT state variables, one needs to integrate both sides over the corresponding dual grid facets crossed by the equivalent current

$$\begin{pmatrix} \widehat{\widehat{\mathbf{j}}}_{e,u} \\ \widehat{\widehat{\mathbf{j}}}_{e,v} \\ \widehat{\widehat{\mathbf{j}}}_{e,w} \end{pmatrix} = \begin{pmatrix} \widehat{\mathbf{h}}_w \\ \mathbf{0} \\ -\widehat{\mathbf{h}}_u \end{pmatrix}. \tag{39}$$

It should be noticed that in the derivation of the above relation the delta function removes the integration along v, whereas the remaining integral along the tangential direction yields the FIT magnetic voltage variables $\widehat{\mathbf{h}}$. Repeating the same procedure for the other components and for both different orientations of the Huygens surface, (36),(37) can be written in a matrix form

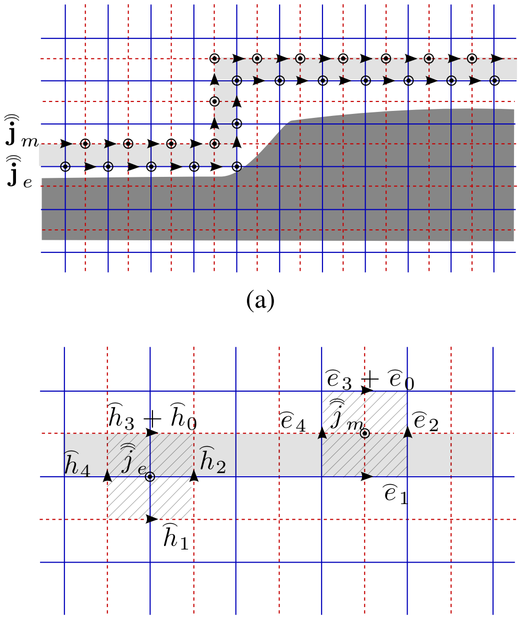

(a)

(b)

Fig. 5. Realisation of the equivalent sources formulation in the FIT grid: (a) electric and magnetic current distributions on the surfaces associated with the primary and dual grid respectively, (b) application of the Faraday and Ampere laws in a primary and a dual grid cell intersected by the corresponding boundary surfaces.

$$\widehat{\widehat{\mathbf{j}}}_e = \mathbf{N}\widehat{\mathbf{h}}_0 \tag{40}$$

$$\widehat{\widehat{\mathbf{j}}}_m = -\mathbf{N}\widehat{\mathbf{e}}_0, \tag{41}$$

with the matrix operator $\mathbf{N}$ being defined as

$$\mathbf{N} = \begin{pmatrix} \mathbf{0} & \mathbf{0} & \mathbf{s}_v \\ \mathbf{0} & \mathbf{0} & -\mathbf{s}_u \\ -\mathbf{s}_v & \mathbf{s}_u & \mathbf{0} \end{pmatrix} \tag{42}$$

with $\mathbf{s}_u = \operatorname{diag}\left[\operatorname{sgn}(\mathbf{n}_i \cdot \hat{u})\right]$, $\mathbf{n}_i$ being the normal to the Huygens surface vector at the ith grid point.

The above definition of the equivalent currents has been based on the classical theory of the induction equivalent for the continuous case [35]. The same relation can be also derived by considering the Maxwell grid equations locally, at a cell level. Let us consider for example the shaded primary cell in Fig. 5. Application of the Faraday's law in this cell yields

$$\widehat{e}_1 + \widehat{e}_2 - (\widehat{e}_3 + \widehat{e}_0) - \widehat{e}_4 = -\widehat{\widehat{j}}_m \tag{43}$$

where we have split the total electric field at the upper part of the cell to the source field contribution in the free space $\widehat{e}_0$ and the scattered field contribution $\widehat{e}_3$. Bringing the source field term in the right hand side and taking into account the Huygens' surface orientation $s_v = 1$, we obtain

$$\widehat{e}_1 + \widehat{e}_2 - \widehat{e}_3 - \widehat{e}_4 = -\widehat{\widehat{j}}_m + s_v \widehat{e}_0. \tag{44}$$

Repeating the same procedure for all the cells crossing the Huygens surface and taking into account both possible orientations of the latter we arrive at the following relation

$$\mathbf{C}\widehat{\mathbf{e}} = -\widehat{\widehat{\mathbf{j}}}_m + \mathbf{N}\widehat{\mathbf{e}}_0. \tag{45}$$

In the same fashion we obtain for the Ampère's law

$$\widetilde{\mathbf{C}}\widehat{\mathbf{h}} = \widehat{\widehat{\mathbf{j}}}_e - \mathbf{N}\widehat{\mathbf{h}}_0. \tag{46}$$

Comparison of (45),(46) with (1),(2) yields the equivalent currents definition of (40),(41).

An additional advantage of the above approach is that $\widehat{\mathbf{e}}_0$ and $\widehat{\mathbf{h}}_0$, being the electric and magnetic field in the free space, are obtained by direct application of the Biot-Savart's integral. This integral can be evaluated semi-analytically for coils of arbitrarily complex shapes via a modal approach as shown in [36].

IV. CALCULATION OF THE IMPEDANCE VARIATION

A scalar observable of great importance for non-destructive testing (NDT) applications is the variation of the self Z (in cases of single coil measurements) or mutual impedance M (for driver pick-up configurations) owing to the presence of structural anomalies in the geometry of the inspected work-piece. These anomalies can are related to material defects such as corrosion pitting or cracking or to variations in the piece profile as edges corners, holes etc.

Let us consider a two-coil driver-pickup configuration. The mutual impedance of the two coils can be written as

$$M(u_c, v_c) = M_0 + \Delta M(u_c, v_c) \tag{47}$$

where M_0 is the mutual impedance value in the free space and ΔM stands for the variation due to the presence of the piece. Notice that the latter depends on the coils position (u_c, v_c) (both coils are considered to be mounted on a rigid probe and hence their position is described by a single pair of coordinates). The calculation of ΔM can be carried out in a very efficient way via the reciprocity theorem, which for the case of a two coils configuration reads [28]:

$$\Delta M_{12} = \frac{1}{\mu_0 I_1 I_2} \oint\limits_{\partial V} \left[\mathbf{E}_0 \times \mathbf{B} - \mathbf{E} \times \mathbf{B}_0\right] \cdot \mathbf{n} dS \tag{48}$$

where $\mathbf{E}_0, \mathbf{B}_0$ is the electric field and the magnetic flux density induced by the first coil in the free space, when it is fed with harmonic current equal to I_1 ($I_2 = 0$), $\mathbf{E}, \mathbf{B}$ stand for the field solution of the problem in the presence of the piece when only the second coil is excited with current I_2 ($I_1 = 0$), and ∂V is any closed boundary that encloses the conducting work-piece (but not the probe). The unit vector $\mathbf{n}$ stands for the outwards normal to the surface ∂V as in the previous section. Choosing the ∂V boundary to be the same with the Huygens surface [1] and applying the circular shift rule of the scalar triple product, (48) can be written as

$$\Delta M = \frac{1}{\mu_0 I_1 I_2} \oint\limits_{\partial V} \left[(\mathbf{n} \times \mathbf{E}_0) \cdot \mathbf{B} + (\mathbf{n} \times \mathbf{B}_0) \cdot \mathbf{E}\right] dS, \tag{49}$$

which taking into account the equivalent current definition relations (36),(37) becomes

$$\Delta M = -\frac{1}{I_1 I_2} \oint\limits_{\partial V} \left(\mathbf{M} \cdot \mathbf{H} - \mathbf{J} \cdot \mathbf{E}\right) dS. \tag{50}$$

Application of (50) into FIT grid space and taking into account the decomposition along the w direction (10) yields

$$\Delta M = -\frac{1}{\mu_0 I_1 I_2} \sum_{n=-N}^{N} \left(\widehat{\widehat{\mathbf{j}}}_{m,-n} \cdot \widehat{\mathbf{h}}_n - \widehat{\widehat{\mathbf{j}}}_{e,-n} \cdot \widehat{\mathbf{e}}_n\right), \tag{51}$$

where $\widehat{\mathbf{e}}_n, \widehat{\mathbf{h}}_n$ are the electric and magnetic grid voltages obtained for the mode n, respectively, and $\widehat{\widehat{\mathbf{j}}}_{e,-n}, \widehat{\widehat{\mathbf{j}}}_{m,-n}$ stand for the equivalent electric and magnetic currents at the Huygens' surface for the mode $-n$. The above equation is nothing more than the Parserval's theorem in the discrete FIT solution space. Notice that although in theory one has to consider an infinity of modes, the above sum involves modes up to N, following the truncation criterion discussed in section II.

V. NUMERICAL RESULTS

A. Comparison with reference results and performance studies

The numerical performance of the proposed formulation is tested by solving the problem of the eddy current inspection of a conducting piece near a discontinuity. Two different configurations are considered, which correspond to the two symmetries of interest: an infinitely long plate edge (with translational symmetry) and a cylindrical borehole (rotationally symmetric).

The first inspection scenario is depicted in Fig. 6. The considered configuration is the same with the one examined in [3], whose results were taken as a reference. The piece is considered infinite along the parallel to the edge direction, and its thickness is assumed several times greater than the skin depth at the operating frequency in order that the interaction of the induced currents with the lower interface to be negligible.

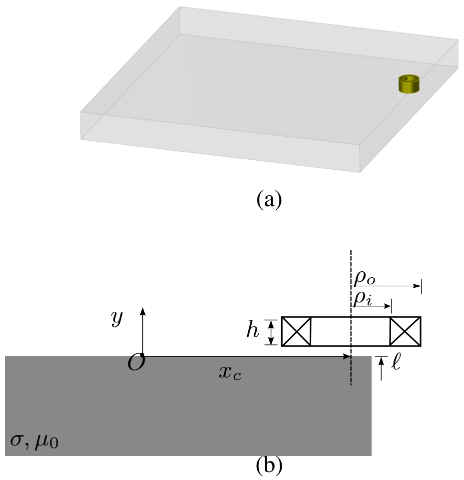

(a)

(b)

Fig. 6. Plate edge inspection with a cylindrical coil: (a) 3D view (b) cross-section.

---

[1] In fact to avoid numerical issues, it is safer to consider an integration surface one grid cell apart from the Huygens' surface.

The piece conductivity is taken equal to $\sigma = 35.4$ MS/m and is assumed non-magnetic. The coil inner and outer radius is $\rho_i = 5$ mm and $\rho_o = 10$ mm, respectively, its length is $h = 5$ mm and is wound with $N = 2500$ turns. The coil is moving parallel to the piece surface at a constant lift-off equal to 2 mm. The inspection is carried out at frequency equal to $f = 1$ kHz, which upon application of the relation $\delta = 1/\sqrt{\pi f \mu_0 \sigma}$ for the skin depth in a half-space, with μ_0 standing for the permeability of the free space, yields $\delta = 2.675$ mm. The piece thickness is taken equal to 10 mm, which makes approximately 4 times the skin depth value, hence it satisfies the half-space approximation.

The results for the probe impedance variation $\Delta Z = Z - jX_0$, where Z is the coil impedance and X_0 stands for the free-space reactance, obtained using the presented approach, are compared with the semi-analytical calculations presented in [3] and with 3D FEM simulations carried out using the COMSOL platform [37]. The comparison for the real and imaginary part of ΔZ as a function of the coil displacement x_c are shown in Fig. 7. For the sake of numerical convenience, both results have been normalised with X_0, which for the given coil geometry and inspection frequency is equal to $X_0 = 500.51\ \Omega$.

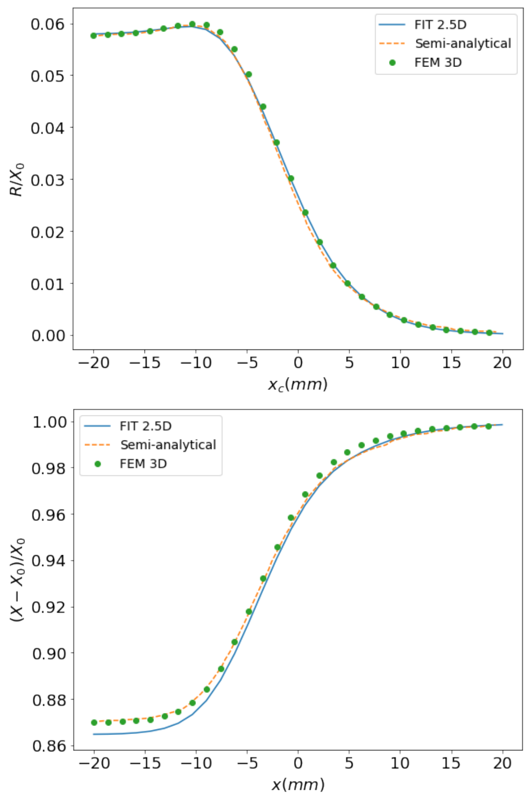

Fig. 7. Real ΔR and imaginary part ΔX of the coil impedance variation as a function of its x_c position (scan displacement). The solid line stands for the results obtained using the presented mixed spatial-spectral approach (referred to as FIT 2.5D), whereas the doted line represents the semi-analytical (reference) solution. Both results are normalised by the coil free space reactance X_0.

For the specific example, a discretisation with 178705 gird nodes and 10 modes along the symmetry axis has been applied. The total calculation for a number of 30 scanning positions reached 351 s, which makes coarsely 12 s per scan point in an average PC with an Intel(R) Core(TM) i7-8850H processor at 2.6 GHz and 32 GB of RAM. For comparison, the corresponding computational time for the 3D FEM solution reached 3925 s in total, which yields 131 s per position. The FEM mesh comprised 516353 degrees of freedom.

It should be noticed at this point that the reduced size of the FIT system of (24), consequence of restricting the spatial discretisation in the transversal $u - v$ plane, allows us to apply direct inversion via LU decomposition. The benefit of addressing to direct solver is that one can treat more than one scan points simultaneously. It is recalled here that each scan point requires the solution of a new numerical problem since the source term at the right hand side is different. This is a particularly important feature for applications involving moving sources as is the case of eddy current nondestructive simulations. A second advantage of this decomposition, in combination with the indirect modelling approach of the sources via the application of the Huygens principle, is that there is no need to re-mesh the problem for each coil position. The source is always represented by the equivalent current distribution on the Huygens surface, which itself does not move. Practically, there is an upper limit concerning the number of scan points that can be treated simultaneously, which is dictated by the available memory.

The second problem deals with the eddy current testing of a cylindrical hole in a conducting non-magnetic half-space, as shown in Fig. 8. The geometry of the piece is this time rotationally symmetric. The considered configuration is the one proposed in [38]. The piece conductivity is taken equal to $\sigma = 24.36$ MS/m. The coil dimensions in this case are $\rho_i = 6.95$ mm, $\rho_o = 9.35$ mm and $h = 6.7$ mm and its number of turns is $N = 335$. The coil scans the tube at a constant radial position equal to $\rho_c = 5.63$ mm with its axis being normal to the tube walls. The inspection frequency is $f = 10$ kHz, which implies a skin depth equal to $\delta = 0.32$ mm. As underlined in the previous example, the thickness of the conducting part along the radial direction should be taken several times greater than δ in order to satisfy the assumption of an infinitely thick piece. For the present calculation, the piece thickness was taken equal to 80 mm, which largely satisfies the above constrain.

The comparison of the calculated probe impedance variation ΔZ with the experimental results provided in [38] is given in Fig. 9. Both results are normalised with respect to the free space reactance, which for the given inspection frequency reads $X_0 = 110.08\ \Omega$.

The numerical results of Fig. 9 were obtained using the same computer with the previous example. The spatial mesh consisted of $2.8\ 10^5$ nodes and 15 modes were considered for the spectral representation in the azimuthal variation. The total calculation time for 15 scanning positions was 832 s.

B. Computational cost

The overall computational burden of the solution (if we neglect the time needed for the computation of the material

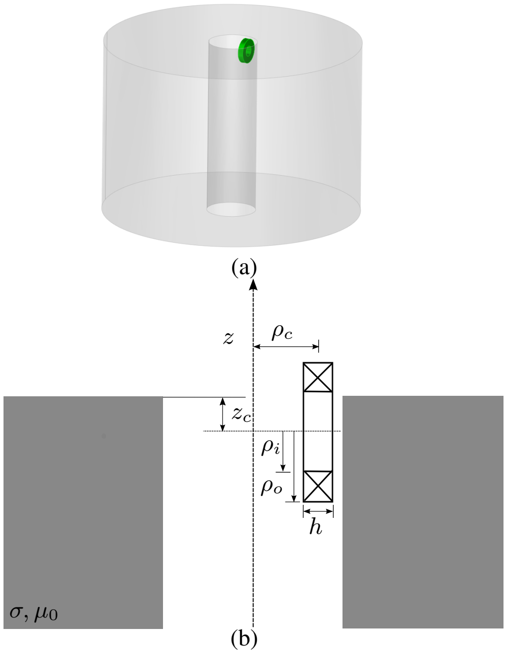

Fig. 8. Plate edge inspection with a cylindrical coil: (a) 3D view (b) cross-section.

matrices and the system assembly) is mainly determined by the number of nodes in the discretisation $u - v$ plane, $3N_d$, the number of modes along the symmetry axis, N_m, and the number of right-hand-side vectors (i.e. the number of independent sources and/or the positions in the case of a moving source), N_s.

Since the solution for each mode is independent from another, the computational time scales linearly with the number of considered modes, N_m, if the system is inverted using a single-core machine. Passing the system to a CPU/GPU parallel architecture, a speed-up equal to the number of parallel processes, with a theoretical maximum the number of modes, N_m, can be achieved.

The scaling with respect to the other two parameters, namely the nodes of the 2D grid, N_d, and the number of sources, N_s, is determined by the corresponding scaling factors for the LU decomposition for sparse systems, and it is less trivial to determine theoretically since it depends to a number of factors, among them on implementation details. We can use the known formulas for a full systems in order to set an upper limit of the computational time of the method and use this formula as a guideline for the derivation of an heuristic approximation based on numerical experiments.

Assuming thus that the system was full, the computational time per mode would be given by the following formula

$$T_{sim}/T_f = 2/3N_d^3 + 2N_d^2 N_s \tag{52}$$

where the first term gives the number of operations for the system factorisation, the second term is the respective number for the forward and backward substitution and T_f stands for the CPU time per flop, which is machine dependent. Based on this relation, we may anticipate that the real computational cost

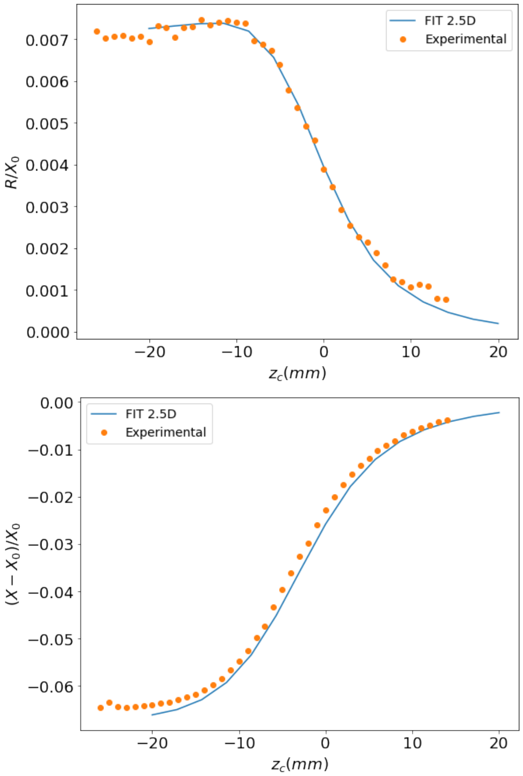

Fig. 9. Calculated results for the real and imaginary part of the coil impedance variation along the scan line vs. measurements. The solid line represents the numerical results obtained with the proposed approach (FIT 2.5) whereas then circular marks stand for the measurements.

for the system at hand should admit an exponential dependence of the general form

$$T_{sim}/T_f = aN_d^{\alpha} + bN_d^{\beta} N_s \tag{53}$$

with a, b constants and α, β exponents that need to be determined, and for which we expect to lie in the intervals $1 \leq \alpha < 3$ and $1 \leq \alpha < 2$. In order to proceed to an estimation of their specific values, the first problem of the previous section, i.e. the scanning coil over the half-space edge, has been solved for a different number of grid nodes and the computational time needed for the system inversion has been measured (the CPU time needed for the construction of the system and the post-processing is not taken into account here). The corresponding plots for different grid sizes and different numbers of coil positions is shown in Fig. 11. The computational time is a linear function of N_s, as expected. All computations have been carried out for a constant number of modes $N_m = 10$.

Calculating the best linear fit to the different datasets, and assuming the dependence of (54), we can associate the the constant term of the fitted polynomials to aN_d^{α}, whereas the linear term coefficients are associated to the bN_d^{β}. The variation of the two coefficients versus N_d in logarithmic scale is shown in

The slope of the two lines in the logarithmic scale will yield the sought approximation of the α and β exponents. We

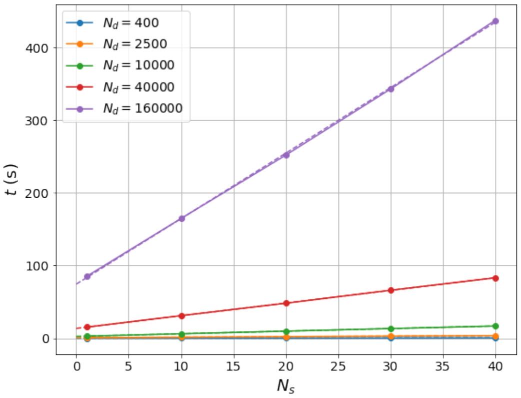

Fig. 10. Simulation time as function of the number of scan positions for a number of different grid resolutions. The time scales almost linearly with the size of the problem as the linear fit results confirm (dashed lines). The considered number of modes is N_m=10.

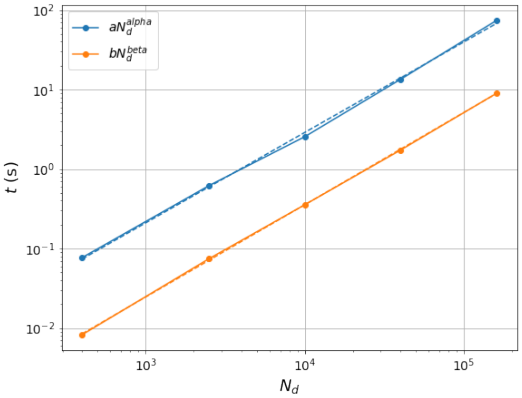

Fig. 11. Coefficients of the fitted polynomial for the curves of Fig. 11 as function of the grid size N_d. The dotted line stands for the best polynomial fit in the logarithmic space.

thus finally obtain for the computational cost the following approximation

$$T_{sim}/T_f = \left(aN_d^{1.14} + bN_d^{1.16}N_s\right)N_m. \tag{54}$$

It must be underlined that the above procedure has been entirely based on a particular example, and it can by no means claim being a rigorous and general method for the derivation of the scaling of the computational time with the solution parameters. It can merely serve as an indicator of the true behaviour. It should be however noticed that a similar trend has been observed for other cases as well. The main conclusion of this study is that the dependence of the computational time is almost linear to the size of the 2D mesh N_d and proportional to N_s and N_m.

VI. DISCUSSION

A mixed spatial-spectral technique was proposed for the solution of the eddy-current induction problem in geometries employing symmetrical work-pieces and arbitrary current sources. The restriction of the spatial discretisation in the transversal to the symmetry axis plane $u - v$, in conjunction with the indirect description of the sources via the equivalence theorem provides an efficient numerical scheme with reduced size. Consequently, LU-based direct solvers can be used for the inversion of the linear system obtained by the application of the spatial grid for a given mode, which allows the simultaneous treatment of different coil positions.

Recalling that local deviations of the material properties from their nominal values (e.g. material defects) can be also expressed in terms of electric and magnetic current sources via the volume equivalence theorem [35], the proposed approach could be extended in order to treat geometries with such anomalies. This is the main idea exploited in the volume integral method [39].

REFERENCES

[1] C. V. Dodd and W. E. Deeds, “Analytical solutions to eddy current probe coil problems,” vol. 39, no. 6, pp. 2829–2838, May 1968.

[2] C. V. Dodd, C. C. Cheng, and W. E. Deeds, “Induction coils coaxial with an arbitrary number of cylindrical conductors,” vol. 45, no. 2, pp. 638–647, Feb. 1974.

[3] T. Theodoulidis and J. R. Bowler, “Interaction of an eddy-current coil with a right-angled conductive wedge,” *IEEE Trans. Magn.*, vol. 46, no. 4, pp. 1034–1042, Apr. 2010.

[4] J. R. Bowler, T. Theodoulidis, and N. Poulakis, “Eddy current probe signals due to a crack at a right-angled corner,” *IEEE Trans. Magn.*, vol. 48, no. 12, pp. 4735–4746, Dec. 2012.

[5] A. Skarlatos and T. Theodoulidis, “Solution to the eddy-current induction problem in a conducting half-space with a vertical cylindrical borehole,” *Proc. R. Soc. London, Ser. A*, vol. 468, no. 2142, pp. 1758–1777, Jun. 2012.

[6] ——, “Calculation of the eddy-current flow around a cylindrical through-hole in a finite-thickness plate,” *IEEE Trans. Magn.*, vol. 51, no. 9, p. 6201507, Sep. 2015.

[7] K. Pipis, A. Skarlatos, T. Theodoros, and D. Lesselier, “ECT-signal calculation of cracks near fastener holes using an integral equation formalism with dedicated Green’s kernel,” *IEEE Trans. Magn.*, vol. 52, no. 4, p. 6200608, Apr. 2016.

[8] A. Skarlatos and T. Theodoulidis, “Analytical treatment of eddy-current induction in a conducting half-space with a cylindrical hole parallel to the surface,” *IEEE Trans. Magn.*, vol. 47, no. 11, pp. 4592–4599, Nov. 2011.

[9] ——, “Semi-analytical calculation of the low-frequency electromagnetic scattering from a near-surface spherical inclusion in a conducting half-space,” *Proc. R. Soc. London, Ser. A*, vol. 470, no. 2170, Jun. 2014.

[10] P. Vafeas, A. Skarlatos, T. Theodoulidis, and D. Lesselier, “Semi–analytical method for the identification of inclusions by air–cored coil interaction in ferromagnetic media,” *Math. Method. Appl. Sci.*, vol. 41, no. 16, pp. 6422–6442, Nov. 2018.

[11] R. Albanese, R. Martone, G. Miano, and G. Rubinacci, “A T formulation for 3D finite element eddy current computation,” *IEEE Trans. Magn.*, vol. 21, no. 6, pp. 2299–2302, Nov. 1985.

[12] O. Bíró and K. Preis, “An edge finite element eddy current formulation using a reduced magnetic and a current vector potential,” *IEEE Trans. Magn.*, vol. 36, no. 5, pp. 3128–3130, Sep. 2000.

[13] O. Bíró, G. Koczka, and K. Preis, “Fast time-domain finite element analysis of 3-D nonlinear time-periodic eddy current problems with T, $\Phi - \Phi$ formulation,” *IEEE Trans. Magn.*, vol. 47, no. 5, pp. 1170–1173, May 2011.

[14] M. Eller, S. Reitzinger, S. Schöps, and S. Zaglmayr, “A symmetric low-frequency stable broadband Maxwell formulation for industrial applications,” *SIAM J. Sci. Comput.*, vol. 39, no. 4, pp. B703–B731, 2017.

[15] T. Weiland, “Time domain electromagnetic field computation with finite difference methods,” *Int. J. Numer. Modell.*, vol. 9, no. 4, pp. 295–319, Jul.-Aug. 1996.

[16] M. Clemens and T. Weiland, “Discrete electromagnetism with the finite integration technique,” *Progress Electromagn. Res. (PIER)*, vol. 32, pp. 65–87, 2001.

[17] R. Schuhmann and T. Weiland, “Conservation of discrete energy and related laws in the finite integration technique,” *Progress Electromagn. Res. (PIER)*, vol. 32, pp. 301–316, 2001.

[18] M. Clemens and T. Weiland, “Magnetic field simulation using conformal FIT formulations,” *IEEE Trans. Magn.*, vol. 38, no. 2, pp. 389–392, Mar. 2002.

[19] A. Vigneron, E. Demaldent, and M. Bonnet, “A multi-step solution algorithm for Maxwell boundary integral equations applied to low-frequency electromagnetic testing of conductive objects,” *IEEE Trans. Magn.*, vol. 52, no. 10, p. 7005208, Oct. 2016.

[20] R. Albanese and G. Rubinacci, “Integral formulation for 3D eddy-current computation using edge elements,” *IEE Proc.-A, Sci. Meas. Technol.*, vol. 135, no. 7, pp. 457–462, 1988.

[21] ——, “Solution of three dimensional eddy current problems by integral and differential methods,” *IEEE Trans. Magn.*, vol. 24, no. 1, pp. 98–101, Jan. 1988.

[22] R. Albanese, G. Rubinacci, A. Tamburrino, S. Ventre, and F. Villone, “A fast 3D eddy currents integral formulation,” *COMPEL*, vol. 20, no. 2, pp. 317–331, 2001.

[23] G. Rubinacci, S. Ventre, F. Villone, and Y. Liu, “Matrix pencil method for estimating parameters of exponentially damped/undamped sinusoid in noise,” *J. Comput. Phys.*, vol. 228, p. 1562–1572, 2009.

[24] G. Rubinacci and A. Tamburrino, “A broadband volume integral formulation based on edge-elements for full-wave analysis of lossy interconnects,” *IEEE Trans. Antennas Propag.*, vol. 54, no. 10, p. 2977–2989, Nov. 2006.

[25] ——, “Automatic treatment of multiply connected regions in integral formulations,” *IEEE Trans. Magn.*, vol. 46, no. 8, p. 2791–2794, Aug. 2010.

[26] T. Weiland, “On the computation of resonant modes in cylindrically symmetric cavities,” *Nucl. Instrum. Methods Phys. Res.*, vol. 216, no. 3, pp. 329–348, Nov. 1983.

[27] A. Skarlatos, R. Schuhmann, and T. Weiland, “Solution of radiation and scattering problems in complex environments using a hybrid finite integration technique - uniform theory of diffraction approach,” *IEEE Trans. Antennas Propag.*, vol. 53, no. 10, pp. 3347–3357, Apr. 2005.

[28] B. A. Auld, F. Muennemann, and D. K. Winslow, “Eddy current probe response to open and closed surface flaws,” *J. Nondestr. Eval.*, vol. 2, no. 1, pp. 1–21, 1981.

[29] J. B. Manges and Z. J. Cendes, “A generalised tree-cotree gauge for magnetic field computation,” *IEEE Trans. Magn.*, vol. 31, no. 3, pp. 1342–1347, May 1995.

[30] P. Hahne and T. Weiland, “3D eddy-current computation in the frequency-domain regarding the displacement current,” *IEEE Trans. Magn.*, vol. 28, no. 2, pp. 1801–1804, Mar. 1992.

[31] M. Clemens and T. Weiland, “Regularization of eddy current formulations using discrete grad-div operators,” *IEEE Trans. Magn.*, vol. 38, no. 2, pp. 569–572, Mar. 2002.

[32] M. Clemens, S. Schöps, H. D. Gersem, and A. Bartel, “Decomposition and regularization of nonlinear anisotropic curl-curl DAEs,” *COMPEL*, vol. 30, no. 6, pp. 1701–1714, 2011.

[33] A. Bossavit, “Stiff problems in eddy-current theory and the regularization of Maxwell’s equations,” *IEEE Trans. Magn.*, vol. 37, no. 5, pp. 3542–3545, Sep. 2001.

[34] O. Bíró and K. Preis, “Finite element analysis of 3-D eddy currents,” *IEEE Trans. Magn.*, vol. 26, no. 2, pp. 418–423, Mar. 1990.

[35] C. A. Balanis, *Advanced Engineering Electromagnetics*. John Willey & Sons, Inc., 1989.

[36] C. Reboud and T. Theodoulidis, “Field computations of inductive sensors with various shapes for semi-analytical ect simulation,” in *Electromagnetic Nondestructive Evaluation (XV)*, ser. Studies in Applied Electromagnetics and Mechanics, B. Rao, T. Jayakumar, K. Balasubramanian, and B. Raj, Eds. Nieuwe Hemweg 6B, 1013 BG Amsterdam, Netherlands: IOS Press BV, 2012, pp. 3–10.

[37] “Comsol multiphysics® v. 5.2,” Stockholm, Sweden. [Online]. Available: www.comsol.com

[38] T. P. Theodoulidis and J. R. Bowler, “Impedance of an induction coil at the opening of a borehole in a conductor,” vol. 103, no. 2, pp. 024 905–1–024 905–9, Jan. 2008.

[39] A. Skarlatos, G. Pichenot, D. Lesselier, M. Lambert, and B. Duchêne, “Electromagnetic modeling of a damaged ferromagnetic metal tube by a volume integral equation formulation,” *IEEE Trans. Magn.*, vol. 44, pp. 623–632, 2008.